Available online at www.sciencedirect.com
ScienceDirect
Cement and Concrete Research 38 (2008) 386–395
Cement and Concrete Research

Shape and size effects on the compressive strength of high-strength concrete

J.R. del Viso, J.R. Carmona, G. Ruiz *

E. T. S. de Ingenieros de Caminos, Canales y Puertos, Universidad de Castilla-La Mancha, 13071 Ciudad Real, Spain

Received 6 February 2007; accepted 13 September 2007

Abstract

In this paper we investigate the influence of the shape and of the size of the specimens on the compressive strength of high-strength concrete. We use cylinders and cubes of different sizes for performing stable stress–strain tests. The tests were performed at a single axial strain rate, $10^{-6}\,s^{-1}$. This value was kept constant throughout the experimental program. Our results show that the post-peak behavior of the cubes is milder than that of the cylinders, which results in a strong energy consumption after the peak. This is consistent with the observation of the crack pattern: The extent of cracking throughout the specimen is denser in the cubes than in the cylinders. Indeed, a main inclined fracture surface is nucleated in cylinders, whereas in cubes we find that lateral sides get spalled leading to the so-called hour-glass failure mode. The remaining cube core gets fragmented due to crushing, in some cases exhibiting a dense columnar cracking in the bulk of the specimen. Finally, we investigate the relationship between the compressive strength given by both types of specimen for several specimen sizes.

Keywords: Concrete compressive strength; Size effect; Specimen shape; High-strength concrete

1. Introduction

By far the most common test carried out on concrete is the compressive strength test. The main reason to understand this fact is that this kind of test is easy and relatively inexpensive to carry out [1]. Testing standard requirements use different geometries of specimens to determine the compressive concrete strength, f_c. The most used geometries are cylinders with a slenderness equal to two and cubes. Shape effect on compression strength has been widely studied and different relationships between the compressive strength obtained for these geometries have been proposed, mainly from a technological standpoint. Such approach eludes the fact that there is a direct relation between the nucleation and propagation of fracture processes and the failure of the specimen. Indeed, experimental observations confirm that a localized microcracked area develops at peak stress [2] or just prior to the peak stress [3]. For this reason compressive failure is suitable to be analyzed by means of Fracture Mechanics.

The failure in uniaxial compression is due to a localization of the damage in a certain zone as it was shown by Van Mier [2]. To study the process of localization in compression he used a method in which the pre-peak deformation was subtracted from the total deformation of the specimen. Later on Markeset and Hillerborg [4] developed a model to study damage localization in compression based on the observations by Van Mier, but added an additional factor, namely the volume energy dissipation, which was mentioned independently by Willam et al. [5] in a conference paper around the same time. Nevertheless, the volume dissipation contribution is rather small. In addition to all that, RILEM TC 148 "Strain Softening of Concrete" focussed the attention on localization in compression. The papers produced by this committee [6,7] show that two effects interact during localization: the slenderness of the samples plus the boundary restraint between the loading platens and the specimen. The first effect, as mentioned above, was observed in 1984 by Van Mier [2]. The second effect was in depth discussed and convincingly shown by Kotsovos [8]. In parallel to the program run by the RILEM TC 148, Van Vliet and Van Mier [9] extended the round robin test program developed by RILEM TC 148 to prisms whose slenderness was between 0.25 and 2.0, and Jansen et al. [10,11] varied the slenderness between 2.0 and 5.5. The results presented

* Corresponding author. ETSI Caminos, C. y P., UCLM. Avda. Camilo José Cela s/n, 13071 Ciudad Real, Spain. Tel.: +34 926 295 398; fax: +34 926 295 391.
E-mail address: gonzalo.ruiz@uclm.es (G. Ruiz).

0008-8846/$ - see front matter © 2007 Elsevier Ltd. All rights reserved.
doi:10.1016/j.cemconres.2007.09.020

in [9] show that by subtracting the elastic deformation from the total deformation, the post-peak stress–deformation curves fall in relatively narrow bands, both for tests conducted between steel platens, and between Teflon platens. This is the same analysis performed by Van Mier [2] who used brush platens and concluded that, irrespective of the type of loading platen, localization of deformations occurs in uniaxial compression. Shah and Sankar [12] obtained similar results after the work by Van Mier, who clearly showed the localization. The localization analysis was completed by papers by Bažant [13] and Hillerborg [14], which were also based on the observations in [2]. Also notable in the field of Fracture Mechanics are the work by Choi et al. [15], on the strain softening in compression under different end constraints and the work of Gerstle [16], where size effect on compressive strength is reported from multiaxial compressive tests. Finally, Borges et al. [17] studied the ductility of concrete in uniaxial and flexural compression. The results of these experimental programs suggest that the compressive test may be considered as a structural test, because the results depend not only on the actual mechanical properties but on the geometry of the specimen and on the boundary conditions, like end constraints, feedback signal or specimen capping [2,9,10,18].

In the last decades concrete technology has made it easier to reach higher strengths and the so-called high-strength concrete (HSC) has appeared as a new construction material. HSC can be that strong that normalized specimens, e.g. 150×300-mm cylinder (diameter×height), may surpass the loading capacity of standard laboratory equipment. To overcome this drawback HSC mixtures are often evaluated using 100×200-mm cylinders, which also meet the requirements of ASTM C39. The strength obtained with this specimen is higher in average than that obtained with 150×300-mm cylinders. This size effect on the compressive strength manifests that the specimen is not behaving as simply as it may seem. Indeed, size effect is understood as the dependence of the nominal strength of a structure on its size (dimension) when compared to another geometrically similar structure [19]. For quasi-brittle materials as concrete, the presence of a non-negligible fracture process zone during the fracture progress, which is commensurate with an internal characteristic length and with the typical size of the material inhomogeneities, provokes a deterministic size effect.

In this paper we investigate the mechanical behavior of HSC (around 100 MPa) tested in a compressive setup in axial strain control. We are particularly interested in the influence of the shape and of the size of the specimens on the compressive strength, f_c, of the material. Based on our results we propose a new relationship between the standard cylinder strength and the strength obtained from cubes of any size.

The article is organized as follows. An outline of the experimental program is given in Section 2. Concrete production and specimens are described in Section 3. In Section 4 we describe the testing procedures. The experimental results are presented and discussed in Section 5. Section 6 includes a simple analysis of size effect and establishes a relationship between the compressive strength measured from standard cylinders and the one obtained from cubes of different sizes. Finally, in Section 7 some conclusions are extracted.

2. Overview of the experimental program

The experimental program was designed to study the size and shape effect on compressive tests performed on high-strength concrete (HSC) specimens. Specifically, we wanted to disclose the influence of the size in cubes and the relationship between compressive strength obtained from standard cylinders, ASTM C39 (100×200 mm) and the strength obtained from cubes. We also intended to analyze the variations in the crack pattern and in the mechanical behavior due to the size and shape of the specimens.

With these intentions in mind, we chose the specimens sketched in Fig. 1. We used cylinders and cubes of different sizes: The dimensions of the cylinders were 75×150 mm and 100×200 mm (diameter×height); the edges of the cubes were 33, 50, 67 and 100 mm long. The dimensions of the cylinders were scaled to the height D, while the dimensions of the cubes were scaled to the edge L, please see Fig. 1. Each specimen was named by a letter indicating the shape, D for cylinders and C for cubes, and one number which indicates the size. For example, D2 names a cylinder of 100×200 mm. We performed at least four tests for each type of specimen.

An important feature of our experimental program — unlike most of the tests available in the scientific literature — consists of providing complete material characterization obtained by independent tests, in many cases performed according to standard recommendations. Specifically, we measured the compressive strength, the tensile strength, the elastic modulus and the fracture energy of the high-strength concrete.

3. Materials and specimens

A single high-strength concrete mix was used throughout the experimental program. It was made with an andesite aggregate of 12 mm maximum size and ASTM type I cement. Microsilica fume slurry and superplasticizer (B-255, BASF) were used in the concrete composition. The water to cement ratio (w/c) was fixed to 0.28.

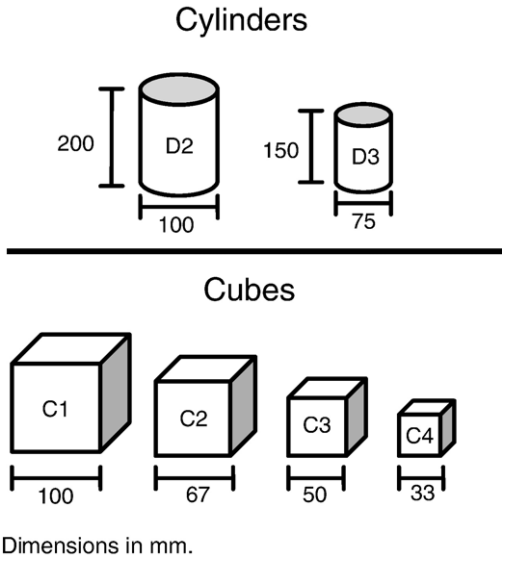

Fig. 1. Specimen geometry.

Table 1
High-strength concrete mechanical properties

	f_c [a]	f_t [b]	E_c	G_F	ℓ_{ch} [c]
	MPa	MPa	GPa	N/m	mm
Mean	89.6	5.4	36.1	119.0	147.3
Std. dev.	7.13	0.6	1.1	13.5	–

[a] Cylinder, compression tests, D2.
[b] Cylinder, splitting tests.
[c] $\ell_{ch} = \frac{E_c G_F}{f_t^2}$.

There was a strict control of the specimen-making process, to minimize scatter in test results. In the case of cylinders the concrete was poured into steel molds in three layers and compacted on a vibration table. In the case of the cubes the specimens were taken by wet-sawing from 100×100×420-mm concrete prisms. The prisms were also made using steel molds and a vibration table. Cylinders and prisms were wrap-cured for 24 h, demolded and stored in a moist chamber at 20 °C and 96% relative humidity. Right after making the cubes from the prisms their sides, as well as the bases of the cylinders, were surface-ground with a wet diamond wheel to ensure perfectly-plane and parallel surfaces. Please, notice that the procedure to get the cubes ensures that the internal structure of the smaller cube, whose edge is only 33 mm long, is exactly the same than that in the other specimens. Of course, the specimens were immediately stored again in the chamber until testing time (six months from concrete making). Just before testing the length, diameter and weight of the cylinders and the edges and weight of the cubes were measured.

Table 1 shows the characteristic mechanical parameters of the high-strength concrete determined in the various characterization tests. In the table, the characteristic length of the concrete, ℓ_{ch}, [20], which is defined as $\ell_{ch}=E_cG_F/f_t^2$, being E_c the elastic modulus, G_F the fracture energy and f_t the tensile strength which we obtain here through splitting tests, is also shown. Please, notice that the characteristic length, ℓ_{ch}, of this concrete is roughly 150 mm, closely half the ℓ_{ch} of normal concrete (ℓ_{ch}=300 mm). This means that, from a Fracture Mechanics standpoint, we expect that our high-strength concrete (HSC) may present a more brittle behavior than a NSC for the same specimen size, since the characteristic length is related with the extension of the fracture process zone [19].

4. Experimental procedures

4.1. Characterization tests

Compressive tests were carried out on 4 cylindrical specimens according to ASTM C39 on 100×200 mm (diameter×height), except for a reduction of the axial displacement rate of the machine actuator, which was 0.018 mm/min.

The elastic modulus was obtained according to ASTM C469 on cylindrical specimens of 150×300 mm. The tests were run under displacement control, at a rate of 0.3 mm/min.

Brazilian tests were also carried out on cylindrical specimens following the procedures recommended by ASTM C496 on 150×300-mm cylinders (diameter×height). The specimen was loaded through plywood strips with a width of 1/6 of the specimen diameter. The velocity of displacement of the machine actuator was 0.18 mm/min.

Stable three-point bend tests on 100×100×420-mm notched beams were carried out to obtain the fracture properties of concrete following the procedures devised by Elices, Guinea and Planas [21–23]. During the tests the beams rested on two rigid-steel cylinders laid on two supports permitting rotation out of the plane of the beam. These supports can roll with negligible friction on the upper face of a very stiff steel beam fastened to the machine frame.

Table 1 shows the characteristic mechanical parameters of the micro-concrete determined in the various characterization tests.

4.2. Testing procedure

All the specimens were tested on a compressive setup as illustrated in Fig. 2. The experiments were performed on an INSTRON 8800 closed-loop servo-hydraulic dynamic testing machine, with a capacity of 1000 kN. The loading platens are made of hardened steel and have polished surfaces. Two linear variable differential transducers (LVDTs), having a calibrated range of ± 2.5 mm, were attached to the upper platen at 180° (please see Fig. 2). These LVDTs were used to measure axial platen-to-platen displacement, δ. The axial deformation referred to in this paper is the average value of the two LVDTs.

For controlling the tests, the signal of the average axial displacement from the LVDTs was chosen. This average signal represents the axial displacement velocity at the center of the loading platen. This type of control impedes snap-back to take place in the σ–ε curves. The axial strain rate is defined as $\dot{\varepsilon}=\dot{\delta}/\Delta$, where $\dot{\delta}$ is the axial platen-to-platen displacement rate and Δ is the initial distance between the top and bottom plane surfaces over the height of the specimen. This axial strain rate was kept constant for all tests having a value of 10^{-6} s^{-1}. The axial displacement rates selected for each specimen are shown in Table 2.

An elastic band was stuck around the specimen, see Fig. 2, (1) to preserve the fragments together for a posterior analysis, and (2) to avoid an interchange of humidity with the environment during the test. The transversal force provoked by this elastic band was negligible.

The load, P, and the axial displacement, δ, were continually monitored and recorded. We used a pair of clip extensometer centered on the specimen in D2 and D3 to measure the displacement in the central part of the specimen in order to get

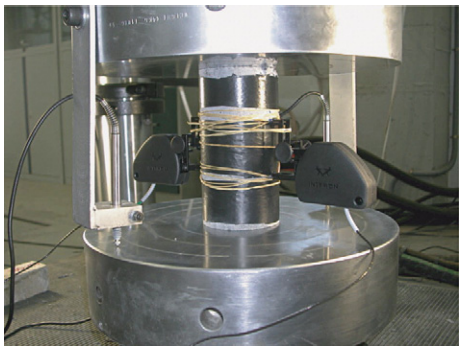

Fig. 2. Testing setup for a D3 specimen.

Table 2
Axial displacement rate for each of the specimens

Denomination	Axial displacement rate, $\dot{\delta}$
	$mm \times min^{-1}$
D2	1.2×10^{-2}
D3	0.9×10^{-2}
C1	0.6×10^{-2}
C2	0.4×10^{-2}
C3	0.3×10^{-3}
C4	0.2×10^{-3}

the elastic modulus. The measurement length was 50 mm. To complete the experimental information, we also took pictures of the crack pattern resulting from each test.

5. Results and discussion

The discussion of the results is organized as follows. First we present and describe the σ–ε curves obtained from the tests. Then we proceed to discuss size effect in cubes and cylinders. Finally the crack patterns are analyzed. Let us emphasize again that cylinders and cubes were tested in strain control keeping constant the axial strain rate throughout the experimental program.

5.1. σ–ε curves

Table 3 lists the average value and the standard deviation for the compressive strength, σ_c, the strain at peak stress, ε_c, the ultimate stress recorded before unstable collapse, σ_u, (in case there was no collapse, it corresponds to the last point recorded in the test), and the corresponding strain, ε_u for all specimens. The strength, σ_c, increases noticeably as the size of the specimen decreases in the case of cubes, whereas for cylinders the effect of the size is almost negligible. The strain at peak load in cubes also increases as size decreases. The ultimate stress and strain are reported to indicate the extension of the softening branch of the curve.

Fig. 3a and b compares σ–ε curves for selected specimens of each size and shape. Specifically, Fig. 3a shows the σ–ε curves obtained for cubes and Fig. 3b for cylinders. The x-axis corresponds to the average strain, i.e. the displacement between the top and bottom plane surfaces over the height of the specimen. The y-axis corresponds to the concrete stress ($\sigma = \frac{P}{\text{Area}}$). A typical σ–ε curve starts with a linear ramp-up. The initial slope shows no significant variations due to the size in the case of cubes while in cylinders the smaller specimen shows a higher slope. In both cases there is a loss of linearity before reaching the peak load, which indicates the initiation of fracture processes.

Table 3
Strength and strain at peak and ultimate load

Specimen		σ_c	ε_c	σ_u	ε_u
		MPa	%	MPa	%
D2	Mean	89.6	0.37	31.4	0.71
	Std. dev.	7.11	0.02	23.31	0.51
D3	Mean	89.9	0.34	41.6	0.22
	Std. dev.	4.65	0.02	22.08	0.42
C1	Mean	96.1	0.57	12.7	1.53
	Std. dev.	1.63	0.01	1.55	0.12
C2	Mean	102.4	0.61	20.9	1.59
	Std. dev.	9.93	0.03	1.81	0.19
C3	Mean	104.2	0.66	38.5	1.46
	Std. dev.	2.19	0.06	6.63	0.13
C4	Mean	110.0	0.85	33.8	1.94
	Std. dev.	7.34	0.09	5.09	0.35

The post-peak behavior depends on the specimen shape. In the case of cylinders, Fig. 3b, a sudden drop in the load takes place after the peak load and there are no significant changes in the softening branch between the scaled tested cylinders. In the case of cubes, Fig. 3a, σ–ε curves show a not so steep softening branch which is associated to a large amount of volumetric energy dissipation, in contrast with the steep softening observed in cylinders.

Fig. 4a compares the relative stress σ/σ_c against ε for scaled cubes. Neither the pre-peak portion of the curves nor the post-peak behavior shows significant variations due to the size. Fig. 4b shows the relative stress versus the inelastic post-peak displacement curves, δ_{inel}, for different scaled cubes. The inelastic post-peak displacement in Fig. 4b, δ_{inel}, was calculated eliminating the elastic component of the displacement as in [2]. We assumed a linear unloading path from the peak stress with a slope equal to that of the pre-peak loading ramp [2]. All the softening branches calculated by this method fail within a narrow band. Nevertheless the fracture energy release grows with the size of the specimen.

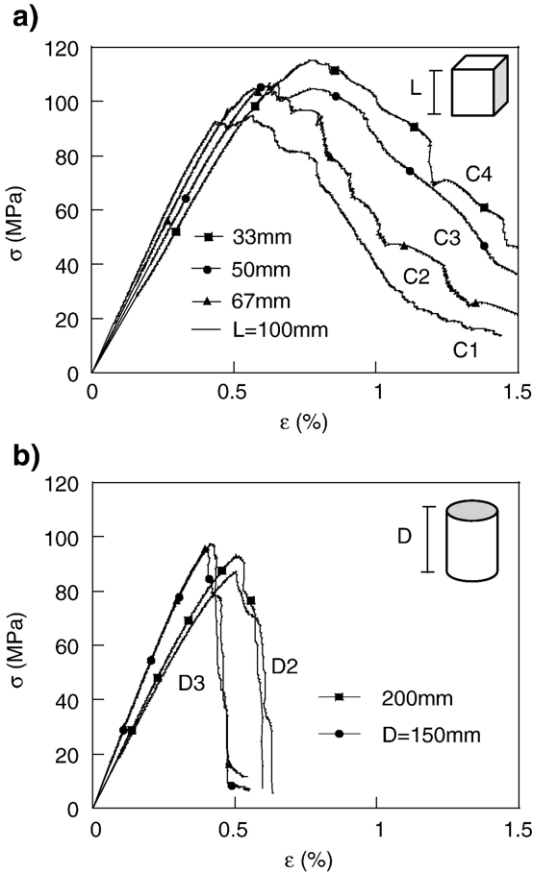

Fig. 3. σ–ε curves corresponding to: (a) cubes; (b) cylinders.

The curves seem to tend to a residual non-zero stress, which could mean that a component due to the aggregate interlocking may appear at the final part of the test.

5.2. Size effect

Fig. 5a and b plots the nominal strength al peak load, σ_N, obtained in the σ–ε curves for the different tested specimens, against a characteristic dimension of the specimen. In Fig. 3a the case of cubes specimens is drawn. It is clearly observed that large specimens resist less in terms of stress than the smaller ones. A interpolation line has been plotted attached to the tests results to facilitate the comparison. Size effect is less noticeable as size increases.

By contrast, the average strength obtained from cylinders is roughly constant within the experimental size interval planned for this research and approximately 10% lower than the horizontal asymptote for the cubes as it can be observed in Fig. 5.

5.3. Crack pattern

The crack pattern observed after the test is sensitive to the shape of the specimen as Fig. 6 shows. A simple visual inspection evidences that the extent of cracking throughout the specimen is denser in the cubes than in the cylinders, please see

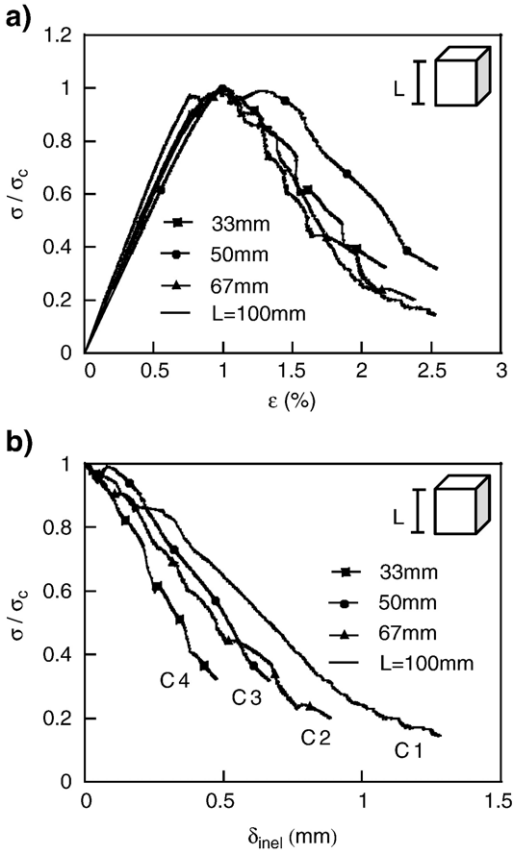

Fig. 4. (a) Relative stress versus ε for scaled cubes; (b) relative stress versus δ_{inel} for scaled cubes.

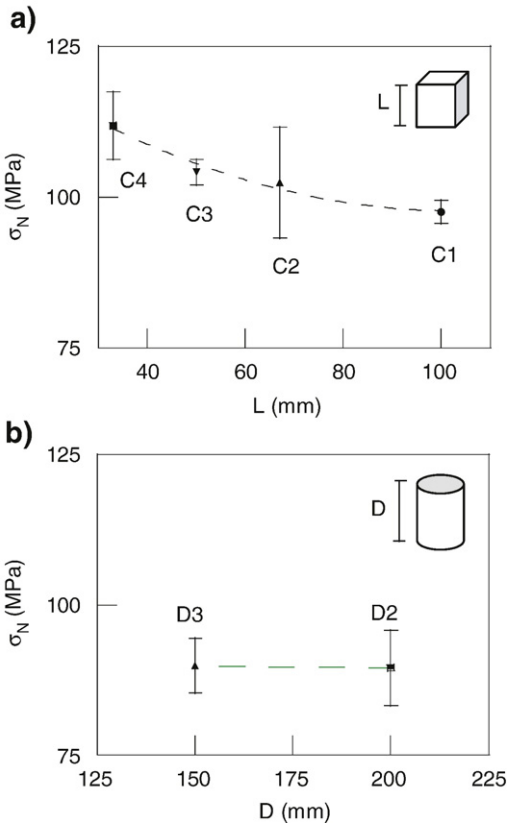

Fig. 5. Size effect on the peak strength: (a) cubes; (b) cylinders.

Figs. 6, 7, 8 and 9. Indeed, a main inclined fracture surface is nucleated in cylinders (Fig. 7), whereas in cubes we find that the lateral sides get spalled leading to the so-called hour-glass failure mode (Figs. 6 and 7). The remaining cube core gets fragmented due to crushing and in some cases exhibits a dense columnar cracking as it is shown in Figs. 8 and 9. This is consistent with the observation made in Section 5.1 about the differences in the σ–ε curves between cubes and cylinders. The steeper response observed in the σ–ε curves for cylinders may be associated to the inclined fracture surface or cone type failure, see Fig. 6, with an initial localization failure in the central part of the specimen. In the case of cubes the fracture process is provoked by a stress concentration near the cube corners. Inclined micro-cracks appear and coalesce near the corners and provoke the crack pattern observed. The stress state inside the cubes provokes crushing and vertical cracks that may end-up forming column-like fragments. The extent of the cracking in this fracture process leads to a higher energy consumption than in the case of cylinders.

Another interesting point is that the failure pattern observed is almost independent for scaled elements in the size interval planned for the experimental program, see Fig. 6. Cylinders broke in all cases by a diagonal fracture plane and cubes present a bursting rupture combined in some cases with a dense columnar cracking. We have also included the crack pattern obtained for a cylinder of 150×300 mm, called D1, in Fig. 6.

6. Relationship between cylinder and cube strength based on Fracture Mechanics theories

In this section we analyze the test results showed in Section 5 within a Fracture Mechanics frame. The aim of this analysis is to get a relationship between cylinder and cube strength valid for cubes of any size. According to Bažant and Planas [19] the maximum load P_c is a function of the specimen geometry (shape and size), boundary conditions and concrete properties. In this investigation only the size and shape are varied, keeping constant the boundary conditions. For the sake of simplicity, the nominal strength at peak load, σ_N, for a concrete specimen is represented by the generalized deterministic energy-based formula for size effect at crack initiation proposed by Bažant [24]. Its applicability is based on the fact the failure is provoked by crack initiation, which is our case as shown in the previous section. So, we can write σ_N as:

$$\sigma_N = \sigma_\infty \left(1 + \frac{B}{\beta_H}\right)^{\frac{1}{r}}; \quad \sigma_\infty = \kappa\sigma_0 \tag{1}$$

where σ_∞ is the theoretical strength for a specimen of infinite size and σ_0 is a reference strength, which in our case we take as the strength that is obtained from the standard test (ASTM C39 on 100×200-mm cylinders). B and κ are empirical constants dependent on the specimen shape and fracture properties of the material, but not on the structural size. Both constants can be obtained from test results. β_H is the denominated Hillerborg's brittleness number [19]. It is defined as the ratio between the representative size of the specimen — represented by the diameter D in the case of cylinders, and L in the case of cubes — and the characteristic length of the concrete, ℓ_{ch}. The values of the exponent r in concrete ranges from 1 to 2 [24] The formulation when the exponent r is equal to 2 is identical to the formula proposed, on the basis of strictly geometric arguments, by Carpinteri et al. [25]. The size effect law can be rewritten as:

$$\sigma_N = \sigma_\infty \sqrt{1 + \frac{B}{\beta_H}}. \tag{2}$$

Applicability of Eqs. (1) and (2) requires not only that the specimens are scaled to each other, but also that the shape of cracks patterns be similar. In our case the crack patterns for cubes of different sizes are very similar, as we showed in Section 5.3.

Fig. 10a shows the linear regression made with the cubes to get the constants κ and B. Please note that the Pearson's correlation coefficient, R in Fig. 10a, is close to 1. Fig. 10b shows the test results compared to the obtained size effect law in

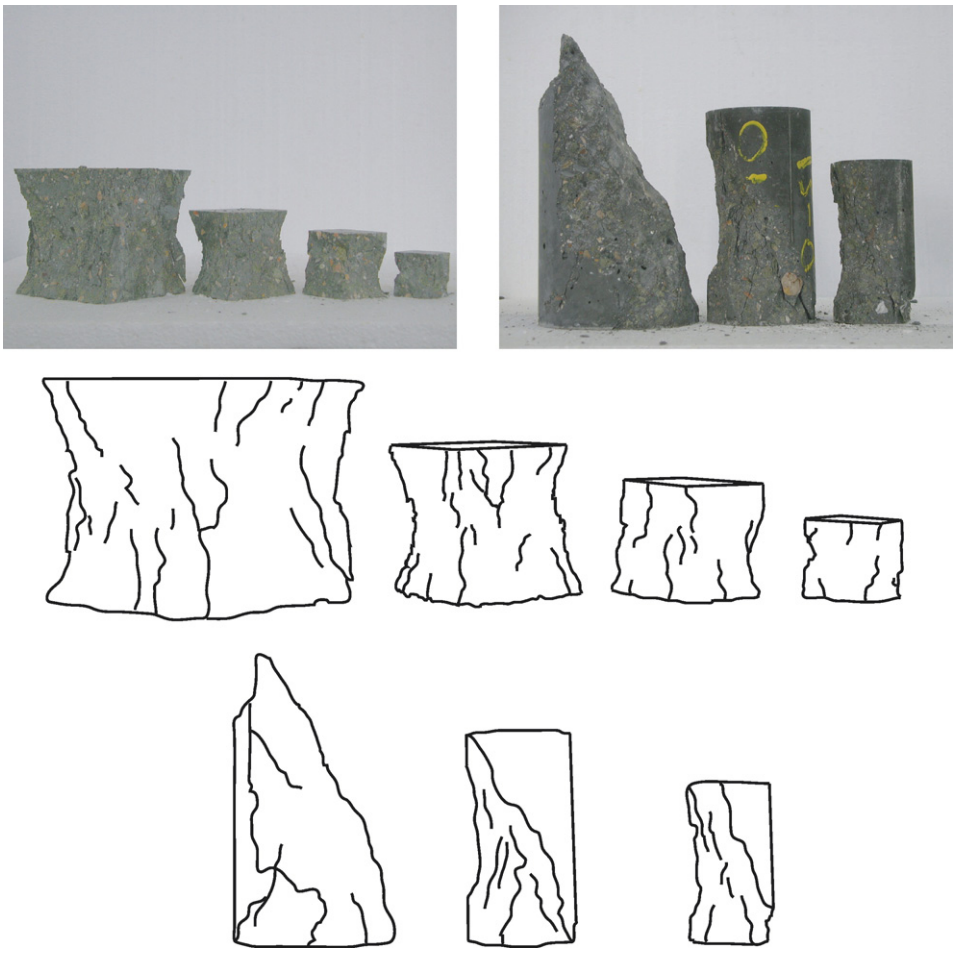

Fig. 6. Crack pattern for cubes and for cylinders.

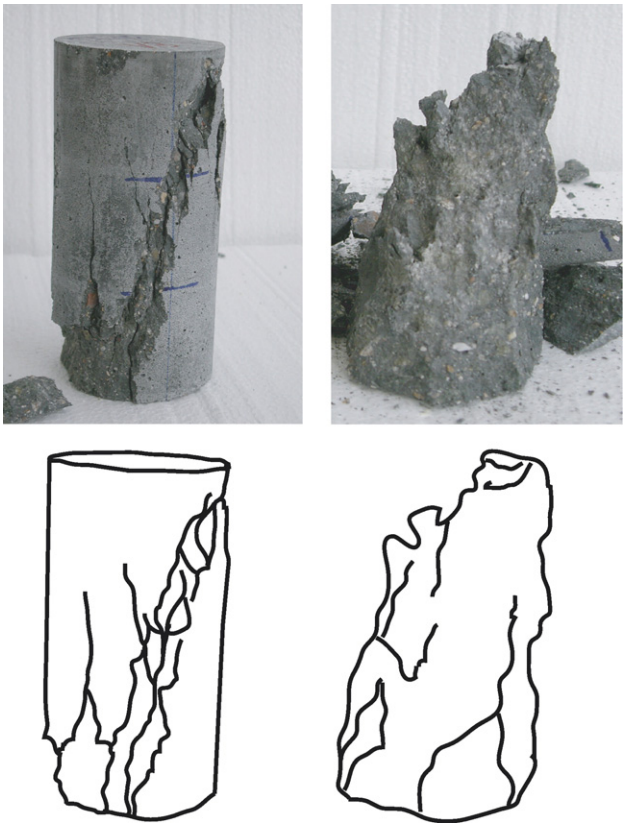

Fig. 7. Main inclined fracture nucleated in a 150-mm-tall cylinder.

a non-dimensional fashion. It may be pointed out that size effect tends to disappear when $L \rightarrow \infty$. The compressive strength converges to a value that in our case is quite similar to 1, that is, for big sizes the compressive strength in cubes converges to the compressive strength obtained with the standard procedure. Further analysis would be necessary to evaluate the influence of the type of test control, which in our case was done keeping the platen-to-platen velocity constant. The strength for a specimen of infinite size can be evaluated as $\sigma_\infty = \sigma_0 \kappa$. In our case σ_∞ is equal to 91.0 MPa.

Based on the obtained law, a correlation between compressive strength for cubes of any size, σ_{cub}, and for standard tests, f_c, can be derived. For concrete with a characteristic length of 150 mm, like the one used in this research, the expression is:

$$f_c = \sigma_{cub}\sqrt{\frac{L}{L+L_0}} \tag{3}$$

where L is the side of the cube and L_0 is a empirical constant equal to 20 mm in this case.

Fig. 11a shows the proposed conversion coefficient against the edge of the cubic specimen. Please, notice that as the cube size increases the coefficient tends to one. The expression showed in Eq. (3) could be profitably used to determine the standard compressive strength of HSC from cubes.

The range of validity of Eq. (3) depends on the error associated to the determination of ℓ_{ch}, which is shown graphically as a shaded area in Fig. 11b. To evaluate the characteristic length we estimated the value of E_c, G_F and f_t using the relationships for them in the Model Code [26]. The expression to obtain the fracture energy, G_F, depends on the aggregate size, and so ℓ_{ch} also does. The concrete used for this research is marked in the plot by the intersection of the two thick dashed lines. Interestingly, the size of the aggregate given by the plot coincides with the actual one used in the mix. Based on some experimental programs where all concrete properties were obtained from independent tests [27–29] we can figure out that

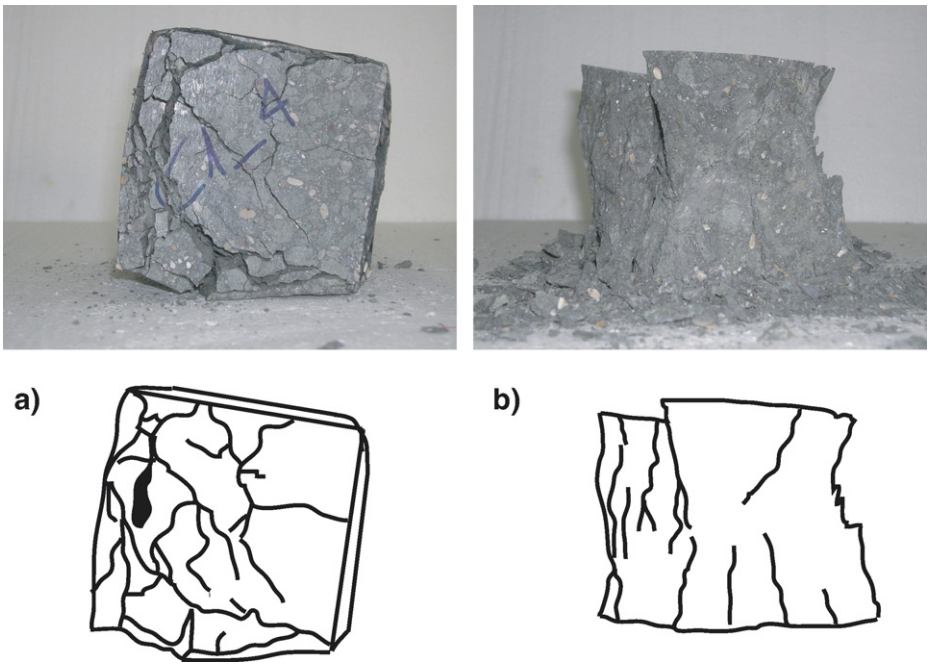

Fig. 8. Tested cubic specimen: (a) view from above; (b) lateral view after unwrapping the specimen.

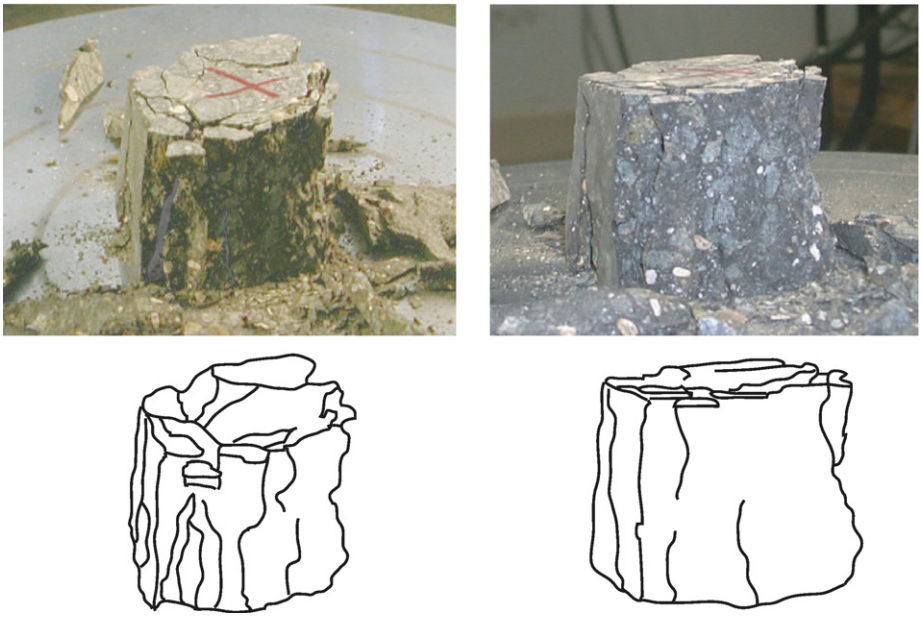

Fig. 9. Columnar cracking observed in 50-mm edged cubes.

the typical relative error for E_c and f_t is 5% and for G_F is 10%. The relative error is defined as the ratio between 1.96 times the standard deviation and the mean value, where 1.96 corresponds to the quantile at 0.05 (or 0.95) absolute value. With these results we obtain a 25% relative error for the characteristic length. The shaded area in Fig. 11b represents the zone where there exists an error of 25% in the value of the estimated

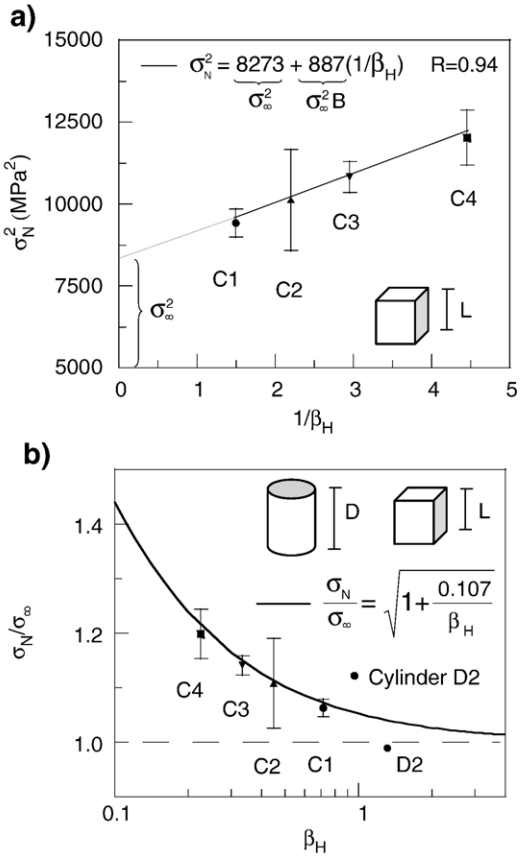

Fig. 10. Size effect in the peak load: (a) results for the regression to calibrate σ_∞ and B coefficients for cubes specimens; (b) size effect law.

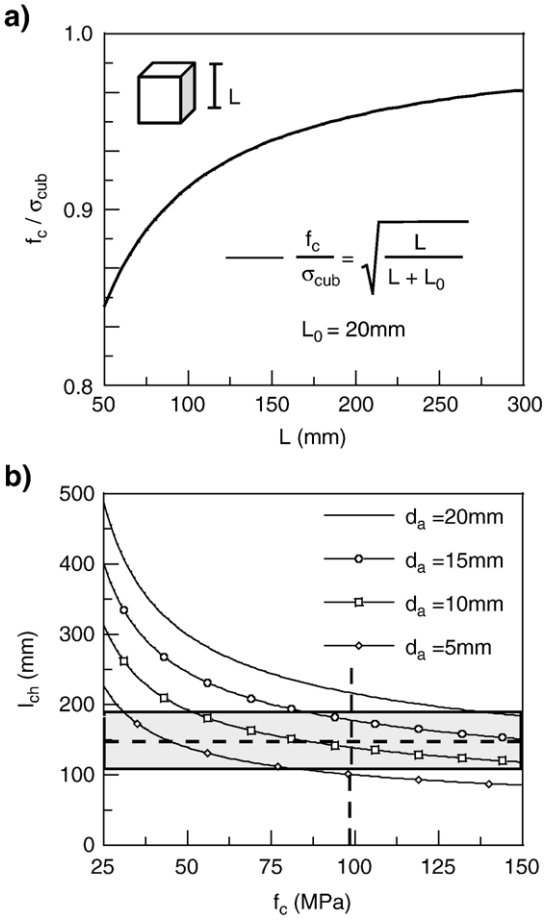

Fig. 11. (a) Relationship between standard compressive strength and cubes size; (b) validation range for the proposed formulation.

compressive strength. Eq. (3) could be used in this interval with a small error.

The fact that cubes are somehow easier to test, since cubes provide directly two couples of perfectly-plane parallel surfaces and they do not require capping, together with the necessity of using specimens whose strength do not surpass the capacity of standard equipment, suggests that cubes would be a good option for compressive test characterization in HSC. The tendency to prefer cylinder to cubes does not have a solid foundation due to the structural character of the compressive test. There is not a reason to think that cylinders catch concrete compressive behavior better than cubes, since compressive tests depend strongly on many factors other than the actual material properties. With this example we want to show that using Fracture Mechanics theories may provide solutions for concrete technological problems. These solutions may help to understand concrete behavior and structural failures better.

7. Conclusions

In this paper we investigated the mechanical behavior of high-strength concrete (around 100 MPa) in compression and tested in strain control. We were particularly interested in the influence of the shape and the size of the specimens on the compressive strength, f_c, of the material. Cylinders and cubes were tested in strain control at a rate that was kept constant throughout the experimental program. Concrete making and testing procedures were closely controlled to reduce experimental scatter. The following conclusions can be drawn from the study:

(1) The pre-peak and post-peak behaviors in the σ–ε curves are dependent on the specimen size and shape. The slope of the softening branch for cubes is mild in contrast with the steep softening observed in cylinders.
(2) Test results show size effect. Large specimens resist less in terms of stress than the small ones. The size effect in the cubes is quite stronger than in cylinders, where the average strength obtained is roughly constant within the size interval planned for this research.
(3) The crack pattern observed after the test is sensitive to the shape of the specimen. A main inclined fracture surface is nucleated in cylinders, whereas in cubes we find that the lateral sides get spalled and that there is fragmentation due to crushing and, in several cases, a dense columnar cracking in the bulk of the specimen. This is consistent with the differences observed in the σ–ε curves between cubes and cylinders. Interestingly, the failure pattern does not change with the size.
(4) The size effect in the compressive strength of cubes is described by a simple model based on Fracture Mechanics concepts. A relationship between the standard cylinder strength and the strength obtained from cubes of any size is derived. It discloses the influence of the cube dimension and may help to deduce relations between the compressive strength determined from cylinders and cubes, inside a theoretical Fracture Mechanics frame.

Acknowledgements

The authors gratefully acknowledge financial support for this research provided by the *Ministerio de Educación y Ciencia*, Spain, under grant MAT2006-09105, and the *Junta de Comunidades de Castilla-La Mancha*, Spain, under grant PAI05-028. Javier R. del Viso and Jacinto R. Carmona also thank the *Junta de Comunidades de Castilla-La Mancha*, Spain, and the *Fondo Social Europeo* for the fellowships that supported their research activity. Likewise, we would like to thank Prof. José Luiz Sousa for his commentaries on the manuscript.

References

[1] S. Mindess, J.F. Young, D. Darwin, Concrete, Prentice Hall, Pearson Education, Inc. United States of America, 2003.
[2] J.G.M. Van Mier, Strain-softening of concrete under multiaxial loading conditions, PhD thesis, Eindhoven University of Technology, Eindhoven, The Netherlands, 1984.
[3] J.M. Torreti, E.H. Benaija, C. Boulay, Influence of boundary conditions on strain softening in concrete compression tests, Journal of Engineering Mechanics-ASCE 119 (12) (1993) 2369–2384.
[4] G. Markeset, A. Hillerborg, Softening of concrete in compression — localization and size effects, Cement and Concrete Research 25 (4) (1995) 702–708.
[5] Y.H. Lee, K. Willam, H.D. Kang, Experimental observations of concrete behavior under uniaxial compression, in: F.H. Wittmann (Ed.), Fracture Mechanics of Concrete Structures, FRAMCOS-2 Conf. Aedificatio Publishers, Freiburg, Germany, 1995, pp. 397–414.
[6] Strain softening of concrete, Materials and Structures 30 (1997) 195–209.
[7] Strain softening of concrete, Materials and Structures 33 (2000) 347–351.
[8] M.D. Kotsovos, Effect of testing techniques on the post-ultimate behaviour of concrete in compression, Materials and Structures 16 (1983) 3–12.
[9] M.R.A. Van Vliet, J.G.M. Van Mier, Experimental investigation of concrete fracture under uniaxial compression, Mechanics of Cohesive-Frictional Materials 1 (1996) 115–127.
[10] D.C. Jansen, S.P. Shah, E.C. Rossow, Stress–strain results of concrete from circumferential strain feedback control testing, ACI Materials Journal 92 (4) (1995) 419–428.
[11] D.C. Jansen, S.P. Shah, Effect on length on compressive strain softening of concrete, Journal of Engineering Mechanics-ASCE 123 (1) (1997) 25–35.
[12] S.P. Shah, R. Sankar, Internal cracking and strain-softening response of concrete under uniaxial compression, ACI Materials Journal 84 (3) (1987) 200–212.
[13] Z.P. Bažant, Identification of strain-softening constitutive relation from uniaxial tests by series coupling model for localization, Cement and Concrete Research 19 (1989) 973–977.
[14] A. Hillerborg, Fracture mechanics concepts applied to moment capacity and rotational capacity of reinforced concrete beams, Engineering Fracture Mechanics 35 (1–3) (1990) 233–240.
[15] S. Choi, K.C. Thienel, S.P. Shah, Strain softening of concrete in compression under different end constraints, Magazine of Concrete Reseach 48 (175) (1996) 103–115.
[16] K.H. Gerstle, et al., Strength of concrete under multiaxial stress states, Proc. Douglas McHenry International Symposium on Concrete and Concrete Structures, ACI Special Publication SP-55, American Concrete Institute, Detroit, USA, 1978, pp. 103–131.
[17] J.U.A. Borges, K.V. Subramaniam, W.J. Weiss, S.P. Shah, T. Bittencourt, Length effect on ductility of concrete in uniaxial and flexural compression, ACI Structural Journal 101 (6) (2004) 765–772.
[18] S.P. Shah, S.E. Swartz, C. Ouyang, Fracture Mechanics of Concrete, Wiley, New York, 1995.
[19] Z.P. Bažant, J. Planas, Fracture and Size Effect in Concrete and Other Quasibrittle Materials, CRC Press, Boca Raton, 1998.

[20] P.E. Petersson, Crack Growth and Development of Fracture Zones in Plain Concrete and Similar Materials, Report No. TVBM-1006, Division of Building Materials, Lund Institute of Technology, Lund, Sweden, 1981.
[21] G.V. Guinea, J. Planas, M. Elices, Measurement of the fracture energy using three-point bend tests. 1. Influence of experimental procedures, Materials and Structures 25 (1992) 121–128.
[22] M. Elices, G.V. Guinea, J. Planas, Measurement of the fracture energy using three-point bend tests. 3. Influence of the cutting the P–δ tail, Materials and Structures 25 (1992) 327–334.
[23] J. Planas, M. Elices, G.V. Guinea, Measurement of the fracture energy using three-point bend tests. 2. Influence of bulk energy dissipation, Materials and Structures 25 (1992) 305–312.
[24] Z.P. Bažant, Size effect in tensile and compression fracture of concrete structures: Computational modeling and design, in: F.H. Wittmann (Ed.), Fracture Mechanics of Concrete Structures, Aedificatio Publishers, Freiburg, Germany, 1998, pp. 1905–1922.
[25] A. Carpinteri, B. Chiaia, G. Ferro, Size effect on nominal tensile strength of concrete structures: multifractality of material ligaments and dimensional transition from order to disorder, Materials and Structures 28 (1998) 311–317.
[26] CEB-FIP, Model Code 1990, Final Draft, Technical Report 203–205, EFP Lausanne, 1991.
[27] G. Ruiz, M. Elices, J. Planas, Experimental study of fracture of lightly reinforced concrete beams, Materials and Structures 31 (1998) 683–691.
[28] G. Ruiz, J.R. Carmona, Experimental study on the influence of the shape of the cross-section and of the rebar arrangement on the fracture of lightly reinforced beams, Materials and Structures 39 (2006) 343–352.
[29] J.R. Carmona, G. Ruiz, J.R. del Viso, Mixed-mode crack propagation through reinforced concrete, Engineering Fracture Mechanics 74 (2007) 2788–2809.

Glossary

β_H	Hillerborg's brittleness number
δ	axial platen-to-platen displacement
δ_{inel}	inelastic post-peak displacement
$\dot{\delta}$	axial platen-to-platen displacement rate
$\dot{\varepsilon}$	axial strain rate
κ	dimensionless empirical constants
ℓ_{ch}	Hillerborg's characteristic length
σ	average compression stress
σ_0	reference strength
σ_∞	theoretical strength for a specimen of a infinite size
σ_{cub}	compressive strength obtained for cubes
σ_c	peak compression stress
σ_N	nominal strength at peak load
σ_u	ultimate stress recorded
ε	strain
ε_c	strain at peak compression stress
ε_u	ultimate strain recorded
B	dimensionless empirical constants
D	cylinder height
E_c	elastic modulus of concrete
f_t	tensile strength of concrete
f_c	standard compression strength
G_F	fracture energy of concrete
L	cube edge
L_0	empirical constant
P	Load
R	Pearson's correlation coefficient
Δ	initial distance between the top and bottom plates